

Annealing effects on the optical conductivity of single crystal $\text{La}_{1-x}\text{Ca}_x\text{MnO}_3$, ($x=0.1, 0.265$)

O. Ripeka Mercier*

School of Chemical and Physical Sciences, Victoria University of Wellington, P.O. Box 600, Wellington, New Zealand

R. G. Buckley and A. Bittar

Industrial Research Limited, P.O. Box 31-310, Lower Hutt, New Zealand

H. J. Trodahl

School of Chemical and Physical Sciences, Victoria University of Wellington, P.O. Box 600, Wellington, New Zealand

E. M. Haines

IRC Superconductivity, Cambridge University, Cambridge CB3 0HE, United Kingdom

J. B. Metson

Chemistry Department, Auckland University, Private Bag 92019, New Zealand

Y. Tomioka

Joint Research Center for Atom Technology, Tsukuba 305-0046, Japan

(Received 31 October 2000; revised manuscript received 11 April 2001; published 28 June 2001)

Optical reflectance spectra were measured in the temperature range 70–295 K, and in the energy range of 0.006–6 eV for single crystals of $\text{La}_{1-x}\text{Ca}_x\text{MnO}_3$ ($x=0.1, 0.265$) before and after annealing. The conductivity spectrum of the unannealed $\text{La}_{0.735}\text{Ca}_{0.265}\text{MnO}_3$ in its low-temperature metallic phase features a Drude-like peak, the spectral weight of which is dramatically increased by annealing the sample. Annealing also repairs a negative anomaly in the conductivity, which is thought to be associated with a surface layer damaged by polishing. A secondary ion mass spectrometry measurement shows, however, that the surface valence becomes depth dependent upon annealing. On the basis that the skin depth is far greater than the extent of annealing damages in the low-energy spectral region, analysis of the temperature dependence of the effective number of carriers N_{eff} below 0.5 eV is presented.

DOI: 10.1103/PhysRevB.64.035106

PACS number(s): 78.20.Ci, 68.49.Sf, 75.50.Cc, 72.15.Gd

I. INTRODUCTION

The complex magnetic and electronic behavior of the colossal magnetoresistive (CMR) perovskite manganites with the general formula $R_{1-x}A_x\text{MnO}_3$ (R is the trivalent rare-earth ions and A is the divalent alkaline-earth ions) has captured the attention of many and justified extensive study. Material properties are highly tunable, and they exhibit a broad range of electronic and magnetic behaviors with hole doping of alkaline-earth ions onto the rare-earth ion site. The Ca-doped LaMnO_3 has a busy magnetic phase diagram.¹ For $0 < x < 0.2$ the manganites are insulators, with a paramagnetic to ferromagnetic transition upon cooling through $T_c = 160\text{--}180$ K. In the hole-doped range of $0.2 < x < 0.5$, $\text{La}_{1-x}\text{Ca}_x\text{MnO}_3$ undergoes a transition from a paramagnetic insulator (PI) to a ferromagnetic metal (FM) at T_c . The concomitant magnetic and metallic transition has been explained in terms of the double exchange mechanism² and theoretically augmented by incorporating a strong lattice-electron coupling^{3,4} to better explain the magnitude of CMR that is observed at temperatures close to T_c .

Optical conductivity measurements play an important role in determining the electrodynamics of materials, and when made at various temperatures and doping levels, the technique is able to probe electronic correlations and interactions between the lattice and the carriers. A number of studies

have now been published that report the ac conductivity or absorption spectra of manganite single crystals,^{5–14} thin films,^{14,18–21} and polycrystalline^{14,18–21} samples with different dopants (R, A) and levels of hole doping x . The polycrystalline and single-crystal sample studies report different surface-preparation techniques such as polishing,^{5–7,14,18–21} annealing after a polishing treatment,^{11,12} and cleaving.^{8–10} Comparisons between spectra from this array of samples, most of which have been performed on $\text{La}_{1-x}\text{Sr}_x\text{MnO}_3$,^{5,6,8–10,12,15–17} has highlighted the importance of careful sample surface treatments to recover the intrinsic optical reflectivity. Although it is acknowledged that cleaved surfaces present the ideal surface for optical measurements, annealing has been used as an alternative for materials that have no easy cleavage plane. The sensitivity of optical reflection measurements is combated by the use of optical-absorption techniques,^{15–17} which are less susceptible to surface defects.

We have measured the temperature-dependent optical reflectance on single crystals of $\text{La}_{1-x}\text{Ca}_x\text{MnO}_3$ ($x=0.1, 0.265$), first after polishing and second after a well-characterized thermal treatment on the same sample. A secondary ion mass spectrometry (SIMS) measurement to characterize the composition near the sample surface before and after annealing shows that annealing $\text{La}_{1-x}\text{Ca}_x\text{MnO}_3$ alters

the valence near the surface. Although the presence of this surface layer is shown to not significantly affect the quantitative analysis of the optical constants for energies less than 0.5 eV, we venture that the annealing conditions chosen do not fully repair the damage to a sample surface, and that interpretation of data from annealed samples should be attempted with care.

II. EXPERIMENT

Single crystals of $\text{La}_{1-x}\text{Ca}_x\text{MnO}_3$ were grown by the floating-zone method, details of which are published elsewhere.²² Samples at the $x=0.1$ and $x=0.265$ doping levels were polished with 1 μm Al_2O_3 powder and their temperature-dependent reflectance measured. The $x=0.1$ sample was then annealed for 1 h in a flowing O_2 atmosphere at 1000 °C following the procedure of Lee *et al.*¹¹ The thermal treatment opened small cracks on its surface, which may be a symptom of strains being released in the material. Optical measurements were performed on a crack-free region of the surface. The $x=0.265$ sample was annealed at the lower temperature of 650–500 °C for about 30 h. Temperature-dependent reflectance measurements, before and after annealing, were carried out using a Bomem DA8 Fourier-type interferometer (0.006–2 eV) and a grating spectrometer (1–6 eV) at near-normal incidence. The area of the reflecting surfaces were $\pi(1.5 \text{ mm})^2$. An evaporated Au film was used as a reference in the infrared (IR) region and the front reflection from a quartz plate used in the spectral range of 1 to 6 eV. The reflectivity is reproducibly measured to a high photometric accuracy of ± 0.01 in the 0.006–2 eV range. In order to apply the Kramers-Kronig (KK) transform and extract the ac conductivity $\sigma(\omega) = \sigma_1(\omega) + i\sigma_2(\omega)$, the reflectance at the low-energy end of the spectrum was extrapolated to zero frequency using a Hagen-Rubens (HR) dependence for the temperatures of 190 K and below, where the $x=0.265$ sample is in its metallic phase. For the spectra that illustrate the insulating phases ($T > T_c$ for $x=0.265$ and $=0.1$) a constant reflectance was assumed at frequencies less than measured. Between 6 and 37 eV a ω^{-2} extrapolation was used. Beyond 37 eV a ω^{-4} dependence was assumed.

The magnetization was measured before and after annealing each sample to monitor any shifts in T_c . There was a 0.5 K increase in T_c for the $x=0.265$ doped sample, and an increase of approximately 3 K in T_c for the $x=0.1$ doped sample. This rather significant increase of T_c for $x=0.1$ suggests that bulk changes have occurred, something confirmed by the extent of cracking in the sample.

III. RESULTS

A. Effect of annealing on optical constants

The frequency-dependent reflectivity $R(\omega)$ was first measured for the $x=0.1$ doped sample at room temperature, before and after annealing, as illustrated by dashed and solid lines, respectively, in Fig. 1(a). Though not shown, another $R(\omega)$ spectrum taken at 75 K before the sample was annealed is very similar to the 295 K spectrum. The only temperature dependence is exhibited in the expected anharmonic

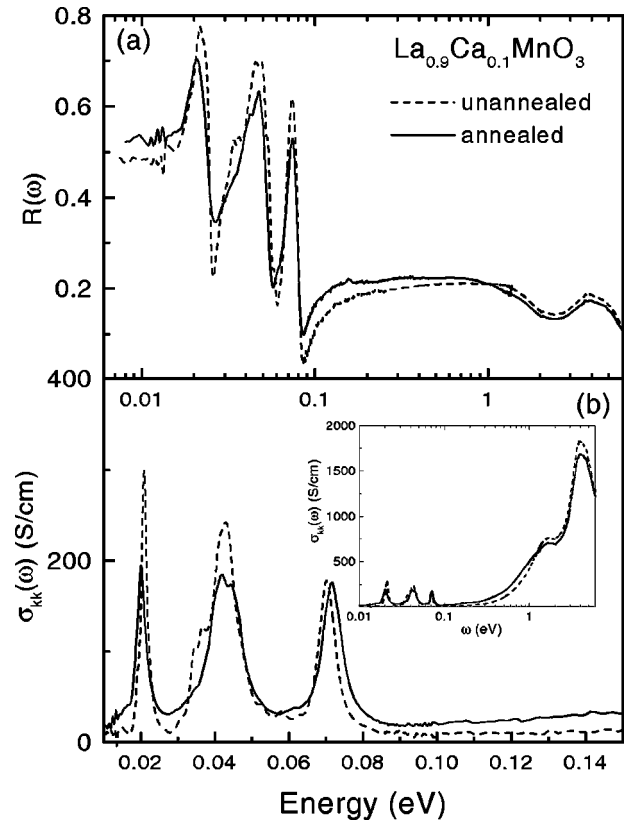


FIG. 1. (a) $R(\omega)$ and (b) $\sigma_{kk}(\omega)$ for unannealed and annealed $\text{La}_{0.9}\text{Ca}_{0.1}\text{MnO}_3$ at 295 K. The inset to (b) shows $\sigma_{kk}(\omega)$ to 5 eV.

broadening and softening of the low-energy optic phonon peaks. It can be seen that there are three phonon modes at low frequency, and in the unannealed sample these are populated with a number of small peaks. These small peaks are not present in the annealed sample, and there is an obvious softening of the mode at $\omega=0.021$ eV. At higher frequencies the spectra are dominated by a very broad midinfrared feature and a peak at ~ 4 eV. The reflectance level has also increased slightly between 0.1 and 0.8 eV, and is decreased in the visible region.

The real part of the KK transform of $R(\omega)$ [hereon labeled as $\sigma_{kk}(\omega)$] for the unannealed and annealed $x=0.1$ sample is illustrated with dashed and solid lines, respectively, in Fig. 1(b). The three peaks displayed in the $\sigma_{kk}(\omega)$ spectra at 0.021, 0.045, and 0.073 eV have been assigned to the “external,” “bending,” and “stretching” modes, respectively.¹⁸ It happens that $\sigma_{kk}(\omega)$ for our annealed $x=0.1$ looks much like the measured spectrum for polycrystalline $x=0.1$,²¹ whereas the irregular spiky phonons of the unannealed $x=0.1$ $\sigma_{kk}(\omega)$ spectrum more closely resemble the published $x=0$ parent compound (LaMnO_3) spectrum.^{9,13,14,21} The $x=0.1$ spectra are in agreement then, but only after annealing. It appears that the thermal treatment chosen has removed imperfections that were evident in the optical spectra as defect modes.

Next, $R(\omega)$ was measured from the $x=0.265$ sample before and after annealing. The higher level of hole doping yields significant temperature dependence in this crystal. The spectra at room temperature and 75 K, before and after an-

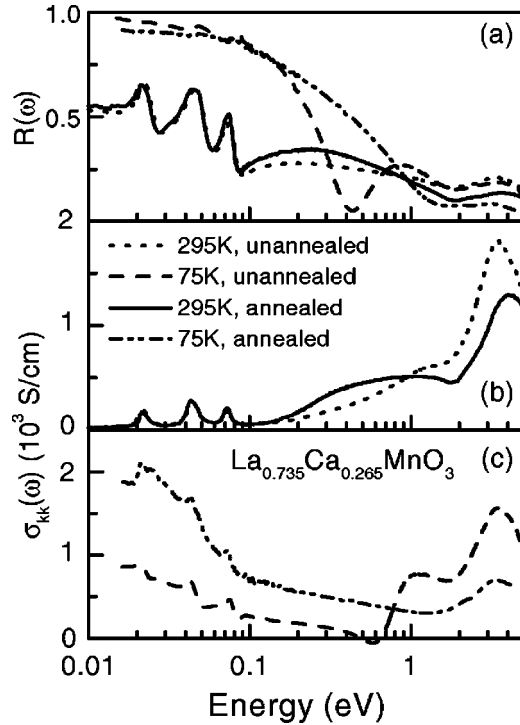


FIG. 2. (a) $R(\omega)$ and $\sigma_{kk}(\omega)$ spectra at (b) 295 K and (c) 75 K for the annealed and unannealed $\text{La}_{0.735}\text{Ca}_{0.265}\text{MnO}_3$. The legend in the middle graph applies to all panels.

nealing, are shown in Fig. 2(a). Examining first the room-temperature data, the three phonon modes that were apparent in the $x=0.1$ sample are readily observed, though the defect modes of the unannealed $x=0.1$ sample spectra are not visible for the sample in either of its unannealed or annealed states. At room temperature the level of $R(\omega)$ for the annealed sample increases in the mid-infrared region between 0.1 and 0.8 eV, but is decreased in the visible region.

These changes are minor, however, in comparison with those seen when the $x=0.265$ sample is in its metallic phase. The energy of the mid-infrared-minimum in the reflectance, or so-called “plasma edge” more than trebles, as it shifts from 0.4 to 1.4 eV on annealing. This is a very similar effect to that seen by Lee *et al.*,¹¹ who found that the plasma edge of single crystal $\text{Nd}_{0.7}\text{Sr}_{0.3}\text{MnO}_3$ (NSMO) shifted from 0.6 to 2 eV upon annealing. Here, this shifted spectral weight absorbs the peak seen in $R(\omega)$ in the unannealed sample at approximately 0.8 eV. The 4-eV peak is still seen in the annealed material, but as for the sample at room temperature, the reflectance level in the visible region has decreased.

The differences that annealing makes are perhaps more obvious in $\sigma_{kk}(\omega)$. The room-temperature spectra in Fig. 2(b) show an increase in the spectral weight of the mid-infrared peak for the annealed sample, though there are relatively small changes in the phonon region.

However, at 75 K the spectrum shows huge changes with annealing. As seen in Fig. 2(c) the apparent $\sigma_{kk}(\omega)$ of the unannealed sample actually goes negative between about 0.5 and 0.6 eV. Clearly a negative $\sigma_{kk}(\omega)$ is unphysical and needs to be addressed. $R(\omega)$ spectra were measured repeatedly, and with different Au reference surfaces, finding varia-

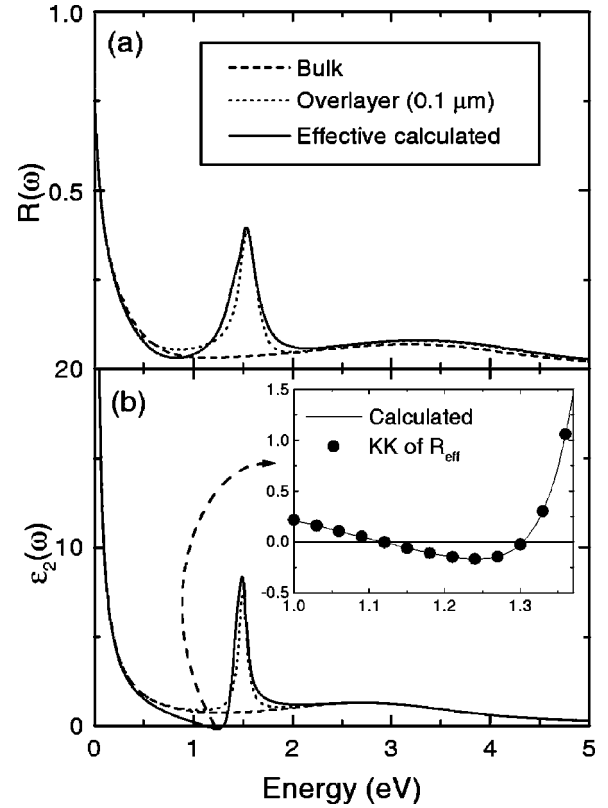


FIG. 3. (a) $R(\omega)$ and (b) $\epsilon_2(\omega)$ for a model material with a 0.1- μm overlayer, demonstrating an effective negative conductivity for an inhomogeneous material. The inset to (b) is a closeup of the 1.2-eV energy region and includes the KK transform of R_{eff} .

tions no greater than our claimed uncertainty. Furthermore, a wide range of both high- and low-energy extrapolations were tried, finding that an unrealistic high-energy extrapolation beyond 5 eV of ω^{-18} was necessary to drive $\sigma_{kk}(\omega)$ positive. It was the negative $\sigma_{kk}(\omega)$ more than anything else which threw doubt on the quality of our polished sample surfaces. It can, in fact, be shown that obtaining a negative σ_{kk} is not such a preposterous result for a sample that is inhomogeneous, and thus violates one of the assumptions made in the KK analysis. To demonstrate this, an effective conductivity was calculated for a bulk material with a 0.1- μm -thickness overlay with slightly different optical features from the bulk. The thickness of the overlay was chosen as a conservative estimate of the extent of polishing damages. Figures 3(a) and 3(b) show $R(\omega)$ and $\epsilon_2(\omega)[=4\pi\sigma_1(\omega)/\omega]$, respectively, in more detail. The bulk $\epsilon_{2b}(\omega)$ (dashed line) comprises a Drude peak with $\omega_p = 1$ eV and $\tau = 1$ eV⁻¹ and a Lorentzian oscillator centered at $\omega_b = 3$ eV. In addition to those oscillators of the bulk the layer has a Lorentzian centered at $\omega_l = 1.5$ eV (dotted line). It can be seen that the calculated apparent conductivity $\epsilon_{2c}(\omega)$ (solid line) from this hybrid material has a distinctly negative component at about 1.2 eV. In addition, the KK transform of the calculated $R(\omega)$ of the hybrid material is shown as solid circles in the inset of Fig. 3(b), which magnifies the region where $\epsilon_2(\omega)$ goes negative. Though not shown in the main panel $\epsilon_{2kk}(\omega) = \epsilon_{2c}(\omega)$ for all ω .

Turning back to our measured spectra in Fig. 2(c), $\sigma_{kk}(\omega)$ for the annealed sample not only remains positive, but the extrapolation at the low-frequency end of the data, which carries a hugely increased spectral weight, yields $\sigma(0) = 2200$ S/cm, rather close to the anticipated value from resistivity measurements on the as-grown sample of $\sigma_{dc} = 2500$ S/cm. The extrapolated zero-frequency conductivity of the unannealed sample was about half this value. The resistivity of the annealed material has not been measured, but it was found by Lee *et al.*¹¹ that the annealing process made very minor changes to $\rho(T)$ in NSMO.

Takenaka *et al.*⁸ have suggested that polishing somehow localizes the carriers. This is why such a large difference in Drude spectral weight is typically seen between polished and cleaved samples in their metallic phase, and a relatively small difference between polished and cleaved spectra for the insulating phases. This suggestion is certainly borne out in our result. It is also shown⁸ in a comparison between cleaved and annealed sample spectra for $\text{La}_{0.825}\text{Sr}_{0.175}\text{MnO}_3$ that annealing only repairs some of the surface damages caused by polishing.

B. Effect of oxygen annealing on surface chemistry

The differences seen in the optical spectra due to annealing naturally led us to a more thorough examination of the sample surface. A SIMS measurement was made [see Figs. 4(a) and 4(b)] on the annealed and unannealed $x=0.265$ sample. The composition variation of La, Ca, Mn, and O ions with depth z below the sample surface is plotted for the $x=0.265$ sample before (a) and after annealing (b). The profiles for each ion have been normalized to their bulk value at $z = 220 \pm 20$ nm.

It can be seen that in the unannealed sample, within uncertainty limits, the composition of the constituent ions is virtually independent of depth. By contrast, in the annealed sample profiles we see significant deviations from the expected bulk compositions for all of the constituent ions near the surface. The La ion in particular is present in quantities of up to 170% of the unannealed sample near the surface. The average percentage for the ions in depths of $0 \leq z \leq 23$ nm is $\text{La}=1.35$, $\text{Ca}=0.91$, $\text{Mn}=0.88$, and $\text{O}=1.12$. The Mn and Ca ion composition deviation is fairly linear, and recovered to 1 (\pm the uncertainty in the data) at approximately $z=190$ nm. For $z \geq 90$ nm the ionic compositions deviate by at most 5%.

Although the optical spectra of the unannealed sample are inconsistent with a single interface, SIMS measurements of this surface [Fig. 4(a)] show no sign of valence differences that could contribute to the unphysical $\sigma(\omega)$. This lends greater credence to the suggestion that strains, not compositional changes, result in a surface layer with a dielectric constant different from the bulk. On the other hand, the SIMS measurement of the annealed $x=0.265$ surface, showing significant disturbances in the valence which persist to depths of $z \approx 30$ nm, prevent us from being entirely confident about presenting our annealed sample spectra as representative of the intrinsic optical properties. The question for these spectra then becomes, how significant are the surface changes from

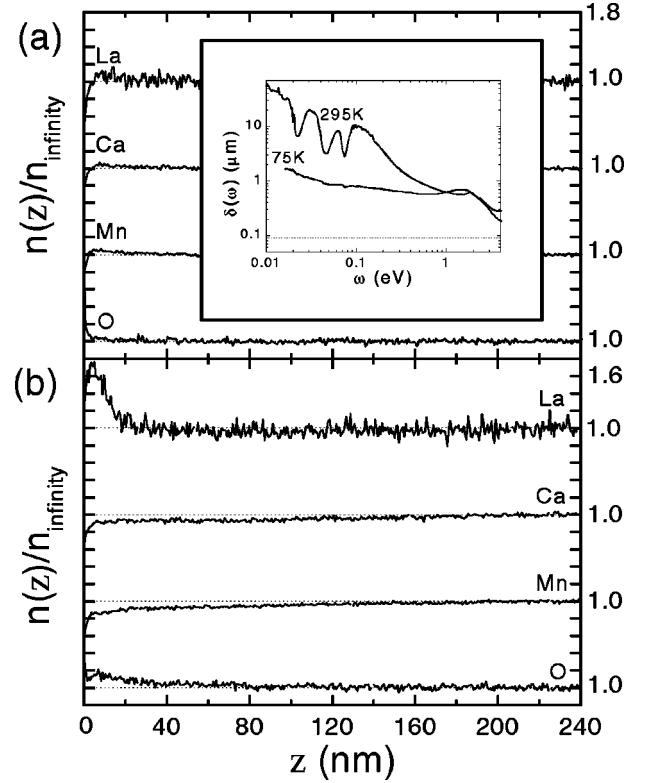


FIG. 4. SIMS atomic composition profiles for (a) unannealed and (b) annealed $\text{La}_{0.735}\text{Ca}_{0.265}\text{MnO}_3$. Horizontal dotted lines at $y = 1$ are a guide to the eye. All y-axis tick marks denote a spacing of 0.2. The inset to panel (a) shows the skin depth $\delta(\omega)$ at 295 and 75 K. The dashed horizontal line denotes the $z = 90$ nm threshold. The profiles obscured by the inset to (a) show behavior no different than that shown.

the point of view of the light being used to probe the material? To answer this question, the skin depth $\delta(\omega)$ for this material was calculated by taking the inverse of the absorption coefficient $\alpha(\omega) = 2\omega k(\omega)/c$. $k(\omega)$ (the imaginary part of the refractive index) is found from the KK transform of the annealed $x=0.265$ sample reflectance. As can be seen in the inset to Fig. 4(a), $\delta(\omega)$, shown at 75 and 295 K, is greater than 90 nm for all of the frequencies at which data were measured. For frequencies less than 1 eV $\delta(\omega)$ is at least 450 nm, or five times the depth to which residual damages extend and 15 times the depth of significant surface damages. Of course, we cannot deduce any information about the strains near the surface from SIMS, but the large increase in Drude spectral weight seems to suggest that these have been mostly relieved. We venture that for the analysis in the following section, which extends to $\omega = 0.5$ eV (where light probes to a minimum depth of $z = 600$ nm), our data are more than adequately representative of the bulk optical properties.

C. $\sigma_{kk}(\omega, T)$ for $\text{La}_{0.735}\text{Ca}_{0.265}\text{MnO}_3$

Figure 5(a) shows $R(\omega)$ measured for the annealed $\text{La}_{0.735}\text{Ca}_{0.265}\text{MnO}_3$ at various temperatures between 75 and 295 K and in the energy range of 0.006–5 eV. Though not

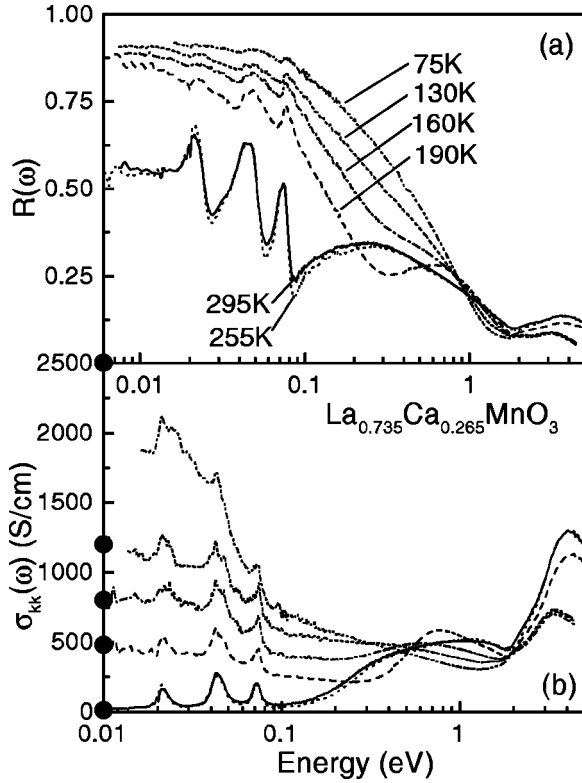


FIG. 5. T -dependent (a) $R(\omega)$ and (b) $\sigma_{kk}(\omega)$ spectra for annealed $\text{La}_{0.735}\text{Ca}_{0.265}\text{MnO}_3$. The line patterns remain the same for both panels.

shown, $R(\omega)$ was also measured in the mid-infrared region at 10 K. The difference between $R(\omega)$ for 75 and 10 K in this spectral region was a few percent. As the temperature is decreased, the three phonon peaks in the far-infrared region become progressively obscured by the increasing low-energy reflectivity background. The magnitude of $R(\omega)$ approaches 1 as ω tends to 0. The reflectance shows strong temperature dependence, even at the 4-eV peak, which displays a shift in energy as well as a change in magnitude. The other interesting features are a peak at about 0.7 eV, seen in the 190 and 160 K spectra, and a broad mid-infrared peak centered at about 1 eV. The 0.7-eV feature is indistinguishable from the 1-eV peak in the spectra above T_c , and if present in $R(\omega)$ for $T < 160$ K it is obscured by the Drude-like background.

The KK transform of the $R(\omega, T)$ spectra are shown in Fig. 5(b) in the energy region 0.01–5 eV. Plotted as solid circles on the y axis are zero-frequency conductivity values deduced from dc resistivity measurements. The sample at 295 and 255 K (i.e., for $T > T_c$) shows a gaplike feature at 0.1 eV. This feature is also seen at this energy in the works of Boris *et al.*⁷ and Kim *et al.*,²⁰ respectively, on single-crystal and polycrystalline samples of approximately a third doped LCMO. The 295 and 255 K spectra are also characterized by two peaks, a broad one at about 1 eV and the other at about 4 eV. The 4-eV peak has been alternately ascribed to the charge-transfer transition between O_{2p} and Mn e_g bands^{11,16,21} and a transition between O_{2p} and Mn t_{2g} bands.^{6,10,14} We find the broad feature at 1 eV near impos-

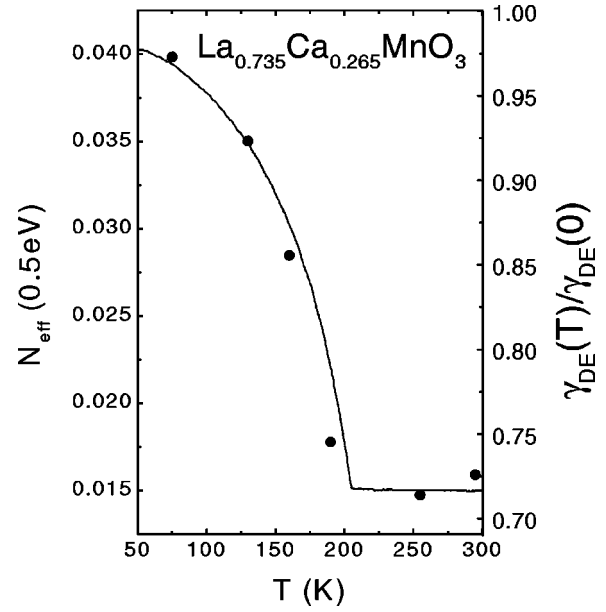


FIG. 6. $N_{eff}(0.5 \text{ eV})$ of the annealed $\text{La}_{0.735}\text{Ca}_{0.265}\text{MnO}_3$ (solid circles) plotted with $\gamma_{DE}(T)/\gamma_{DE}(0)$ (solid line).

sible to fit with just one oscillator, and there is some speculation in the literature as to whether this peak is single.^{11,15}

Below T_c there is a shift in the spectral weight from the mid-infrared to the low-frequency region.²³ This low-frequency Drude-like weight increases further with decreasing temperature and though it somewhat screens the phonon modes, they remain evident, even at the lowest temperature displayed. The broad 1-eV peak seems to transfer some of its weight into the 0.7-eV peak, very prominent in the 190 K spectrum, and the rest to the low-energy Drude peak. The weight and energy of the 0.7-eV peak has decreased at 160 K as the Drude weight further increases, and at lower temperatures there appears to be a clear division of weight: increasing below and decreasing above about 0.5 eV. The temperature dependence of the weight of this Drude-like feature was investigated by evaluating the effective number of carriers N_{eff} for below a cutoff frequency ω_c by using the expression

$$N_{eff}(\omega) = \frac{2mV}{\pi Ne^2} \int_0^{\omega_c} \sigma_1(\omega') d\omega',$$

where m is the electron mass, V is the volume of the unit cell calculated from reported structural data,^{23,24} and N is the number of Mn atoms in this volume. N_{eff} was calculated to $\omega_c = 0.5 \text{ eV}$, a crossover energy below which the Drude weight increases with decreasing temperature and above which the spectral weight decreases as temperature decreases. The temperature dependence of N_{eff} does not change significantly with energy cutoffs $\pm 0.05 \text{ eV}$.

$N_{eff}(T)$, shown as solid circles in Fig. 6, is not proportional to our measurement of the square of the normalized magnetization $[M(T)/M_s]^2$ (not shown) [where $M(T)$ is the magnetization and M_s is the saturated ferromagnetic magnetization at $T=0$], which would be expected in the simple double exchange (DE) picture.²⁵ An absorption¹⁴ study and a

reflectance¹⁰ study demonstrate that the infrared spectral weight associated with the conducting carriers is transferred from the higher-energy transitions in obedience with the scaling relation $1-[M(T)/M_s]^2$ predicted in the DE picture.²⁵ A similar analysis carries large uncertainties for the present data set, as the lesser skin depth for the higher-frequency region probes proportionally more of the damaged surface layer than the bulk. However $N_{eff}(T)$ does scale rather well with a parameter which also incorporates Jahn-Teller (JT) coupling in the DE model. This is the temperature dependent DE bandwidth, $\gamma_{DE}(T)/\gamma_{DE}(0)$ predicted by Kubo and Ohata²⁶ and illustrated as a solid line in Fig. 6. The reason for this good agreement, also seen in other optical studies,^{11,19,20} has been discussed by Kim *et al.*²⁰ in terms of the incorporation of Jahn-Teller (JT) coupling in the DE model, whose Hamiltonian was studied by Röder *et al.*²⁷ However, we have demonstrated that the quantitative interpretation of results of any optical measurement is not independent of surface treatments. A clear picture of the electron dynamics in the $\text{La}_{1-x}\text{Ca}_x\text{MnO}_3$ system is yet to emerge.

IV. CONCLUSIONS

The recent observation that polishing single crystals for optical measurements obscures the intrinsic conductivity suggested that cleaved or annealed surfaces are necessary for overcoming this problem. Our measurements of $\text{La}_{0.735}\text{Ca}_{0.265}\text{MnO}_3$ showed that this polishing damage was extensive enough to return a negative $\sigma_{kk}(\omega)$ for the sample in its metallic phase. A calculation for a modeled bulk and overlayer confirmed that the KK transform can return negative $\sigma_{kk}(\omega)$ for inhomogeneous materials. We anticipated that annealing would heal the surface strains induced by pol-

ishing, and indeed the treatment rescued the $\sigma_{kk}(\omega)$ spectrum for $\text{La}_{0.735}\text{Ca}_{0.265}\text{MnO}_3$ from apparently negative values and produced an increased low-energy spectral weight. However, a SIMS measurement on the sample showed that while its composition before annealing was independent of depth, the composition of the sample surface after annealing differed significantly from that of the bulk, effectively introducing a different type of surface layer. Given that in this case the skin depth of the probing light is many times deeper than the extent of surface disruption we have no hesitation in presenting data on the effective number of carriers up to 0.5 eV from our optical spectra. However, we do suggest that any optical study which uses annealing to release surface strains due to polishing should also be accompanied by a surface characterization measurement, such as SIMS.

It was found that the temperature dependence of N_{eff} scaled well with the predicted temperature-dependent DE bandwidth. This behavior is consistent with the suggestion that Drude metallic behavior in $\text{La}_{0.735}\text{Ca}_{0.265}\text{MnO}_3$ is complicated by electron-phonon interactions. This is in contrast to optical results that appear to confirm the simple DE picture. The central issue for quantitative analysis by reflectivity of bulk crystals appears to be the sample surface treatment.

ACKNOWLEDGMENTS

The author gratefully acknowledges the Foundation for Research into Science and Technology for support. This work was financially supported by a Royal Society of New Zealand Marsden Fund, a Victoria University of Wellington grant, and the New Energy and Industrial Technology Development Organization of Japan.

*Email address: O.Mercier@irl.cri.nz

¹P. Schiffer, A. P. Ramirez, W. Bao, and S.-W. Cheong, Phys. Rev. Lett. **75**, 3336 (1995).

²C. Zener, Phys. Rev. **82**, 403 (1951).

³A. J. Millis, P. B. Littlewood, and B. I. Shraiman, Phys. Rev. Lett. **77**, 175 (1997).

⁴K. Held and D. Vollhardt, Phys. Rev. Lett. **84**, 5168 (2000).

⁵Y. Okimoto, T. Katsufuji, T. Ishikawa, T. Arima, and Y. Tokura, Phys. Rev. Lett. **75**, 109 (1995).

⁶Y. Okimoto, T. Katsufuji, T. Ishikawa, T. Arima, and Y. Tokura, Phys. Rev. B **55**, 4206 (1997).

⁷A. V. Boris, N. N. Koveleva, A. V. Bazhenov, P. J. M. van Bentum, Th. Rasing, S.-W. Cheong, A. V. Samoilov, and N.-C. Yeh, Phys. Rev. B **59**, R697 (1999).

⁸K. Takenaka, Y. Sawaki, and S. Sugai, Phys. Rev. B **60**, 13 011 (1999).

⁹K. Takenaka, K. Iida, Y. Sawaki, S. Sugai, Y. Moritomo, and A. Nakamura, J. Phys. Soc. Jpn. **68**, 1828 (1999).

¹⁰K. Takenaka, Y. Sawaki, R. Shiozaki, and S. Sugai, Phys. Rev. B **62**, 13 864 (2000).

¹¹H. J. Lee, J. H. Jung, Y. S. Lee, J. S. Ahn, T. W. Noh, K. H. Kim, and S.-W. Cheong, Phys. Rev. B **60**, 5251 (1999).

¹²E. Saitoh, A. Asamitsu, Y. Okimoto, and Y. Tokura, J. Phys. Soc. Jpn. **69**, 3614 (2000).

¹³A. Paolone, P. Roy, A. Pimenov, A. Loidl, O. K. Mel'nikov, and A. Ya. Shapiro, Phys. Rev. B **61**, 11 255 (2000).

¹⁴T. Arima and Y. Tokura, J. Phys. Soc. Jpn. **64**, 2488 (1995).

¹⁵Y. Moritomo, A. Machida, K. Matsuda, M. Ichida, and A. Nakamura, Phys. Rev. B **56**, 5088 (1997).

¹⁶M. Quijada, J. Cerne, J. R. Simpson, H. D. Drew, K. H. Ahn, A. J. Millis, R. Shreekala, R. Ramesh, M. Rajeswari, and T. Venkatesan, Phys. Rev. B **58**, 16 093 (1998).

¹⁷J. R. Simpson, H. D. Drew, V. N. Smolyaninova, R. L. Greene, M. C. Robson, Amlan Biswas, and M. Rajeswari, Phys. Rev. B **60**, R16263 (1999).

¹⁸K. H. Kim, J. Y. Gu, H. S. Choi, G. W. Park, and T. W. Noh, Phys. Rev. Lett. **77**, 1877 (1996).

¹⁹K. H. Kim, J. H. Jung, and T. W. Noh, Phys. Rev. Lett. **81**, 1517 (1998).

²⁰K. H. Kim, J. H. Jung, D. J. Eom, T. W. Noh, Jaeyun Yu, and E. J. Choi, Phys. Rev. Lett. **81**, 4983 (1998).

²¹J. H. Jung, K. H. Kim, H. J. Lee, T. W. Noh, E. J. Choi, and Y. Chung, J. Korean Phys. Soc. **31**, L549 (1997).

²²Y. Tokura, A. Urushibara, Y. Moritomo, T. Arima, A. Asamitsu, G. Kido, and N. Furukawa, J. Phys. Soc. Jpn. **63**, 3931 (1994); A. Urushibara, Y. Moritomo, T. Arima, A. Asamitsu, G. Kido, and Y. Tokura, Phys. Rev. B **51**, 14 103 (1995).

²³Q. Huang, A. Santoro, J. W. Lynn, R. W. Erwin, J. A. Borchers,

- J. L. Peng, and R. L. Greene, Phys. Rev. B **55**, 14 987 (1997).
- ²⁴P. G. Radaelli, G. Iannone, M. Marezio, H. Y. Hwang, S-W. Cheong, J. D. Jorgensen, and D. N. Argyriou, Phys. Rev. B **56**, 8265 (1997).
- ²⁵N. Furukawa, J. Phys. Soc. Jpn. **64**, 3164 (1995).
- ²⁶K. Kubo and N. Ohata, J. Phys. Soc. Jpn. **33**, 21 (1972).
- ²⁷H. Röder, J. Zang, and A. R. Bishop, Phys. Rev. Lett. **76**, 1356 (1996).